APPLIED AND ENVIRONMENTAL MICROBIOLOGY, July 2005, p. 4014–4021 Vol. 71, No. 7
0099-2240/05/$08.00+0 doi:10.1128/AEM.71.7.4014–4021.2005

Determination of Spatial Distributions of Zinc and Active Biomass in Microbial Biofilms by Two-Photon Laser Scanning Microscopy

Zhiqiang Hu,[1,2,3] Gabriela Hidalgo,[1] Paul L. Houston,[2] Anthony G. Hay,[3] Michael L. Shuler,[4] Héctor D. Abruña,[2] William C. Ghiorse,[3] and Leonard W. Lion[1]*

School of Civil and Environmental Engineering,[1] Department of Chemistry and Chemical Biology,[2] Department of Microbiology,[3] and School of Chemical and Biomolecular Engineering,[4] Cornell University, Ithaca, New York 14853

Received 23 July 2004/Accepted 30 January 2005

The spatial distributions of zinc, a representative transition metal, and active biomass in bacterial biofilms were determined using two-photon laser scanning microscopy (2P-LSM). Application of 2P-LSM permits analysis of thicker biofilms than are amenable to observation with confocal laser scanning microscopy and also provides selective excitation of a smaller focal volume with greater depth localization. Thin *Escherichia coli* PHL628 biofilms were grown in a minimal mineral salts medium using pyruvate as the carbon and energy source under batch conditions, and thick biofilms were grown in Luria-Bertani medium using a continuous-flow drip system. The biofilms were visualized by 2P-LSM and shown to have heterogeneous structures with dispersed dense cell clusters, rough surfaces, and void spaces. Contrary to homogeneous biofilm model predictions that active biomass would be located predominantly in the outer regions of the biofilm and inactive or dead biomass (biomass debris) in the inner regions, significant active biomass fractions were observed at all depths in biofilms (up to 350 μm) using live/dead fluorescent stains. The active fractions were dependent on biofilm thickness and are attributed to the heterogeneous characteristics of biofilm structures. A zinc-binding fluorochrome (8-hydroxy-5-dimethylsulfoamidoquinoline) was synthesized and used to visualize the spatial location of added Zn within biofilms. Zn was distributed evenly in a thin (12 μm) biofilm but was located only at the surface of thick biofilms, penetrating less than 20 μm after 1 h of exposure. The relatively slow movement of Zn into deeper biofilm layers provides direct evidence in support of the concept that thick biofilms may confer resistance to toxic metal species by binding metals at the biofilm-bulk liquid interface, thereby retarding metal diffusion into the biofilm (G. M. Teitzel and M. R. Park, Appl. Environ. Microbiol. 69:2313–2320, 2003).

Surfaces in both natural and engineered systems are typically colonized by adherent bacteria, resulting in heterogeneous surface coatings (or biofilms) consisting of attached microbial populations and extracellular polymeric substances (EPS) of bacterial origin (4, 7, 9, 13, 14, 42). Biofilm structures consist of aggregated microbial communities embedded with the EPS, which may include complex mixtures of heteropolysaccharides, protein, and nucleic acids (9, 14), separated by a network of open water channels (34). Biofilm formation is dependent on a variety of factors, including surface properties, availability of electron donors and acceptors, microbial species, and hydrodynamics of the surrounding fluid phase (16, 34, 40). Among these variables, microbial species characteristics and the availability of growth substrates play important roles in determining the ultimate spatial distribution of individual organisms in a multiple-species biofilm (31).

If a homogeneous biofilm structure is assumed, it follows that metabolic activity within the deeper layers may be altered because of substrate, oxygen, and/or nutrient limitations. Model simulations based on the assumption of a homogeneous biofilm result in the prediction that active biomass will be located predominantly in the outer regions of biofilms (9, 27, 30, 39). The existence of a heterogeneous structure in which open channels allow the bulk fluid to penetrate to variable depths within biofilms makes conclusions based on the assumption of homogeneous structure of questionable value. Experimental observations are needed to better understand mass transfer of substrate, nutrients, and toxic chemicals into biofilms and to aid in the development of improved biofilm models for environmental and biochemical applications.

Trace metals are ubiquitous, and their interactions with biofilms are of great interest because of the potential role of adherent bacterial populations in the surface chemical reactions that control the phase distribution, bioavailability, and ultimately the biogeochemical cycling of many metal species in natural aquatic systems (21). The availability of both essential and toxic trace metals can also clearly influence the metabolic activities of microorganisms in engineered bioreactors as well as in medical applications (19, 40).

From the physicochemical point of view, biofilms influence the fate of metals both directly, by uptake, adsorption, and complexation (with extracellular metal-binding ligands), and indirectly, through alterations in pH and oxidation/reduction potential, as well as through production of biogenic minerals such as iron and manganese oxides, which strongly bind metals (19, 21). Previous studies of biofilms and metal interactions have demonstrated that metals strongly adsorb to biofilms, at levels significantly greater than those bound by planktonic bacteria of the same strain (12, 42). Nevertheless, the sorption

* Corresponding author. Mailing address: School of Civil and Environmental Engineering, Cornell University, Hollister Hall, Ithaca, NY 14853. Phone: (607) 255-7571. Fax: (607)-255-9004. E-mail: LWL3@cornell.edu.

mechanism for both attached and planktonic bacteria is likely the same; i.e., metal binding with functional groups on extracellular polymers and bacterial cell surfaces, including the amino, carboxylic, hydroxyl, and phosphate groups of (phospho)lipids, proteins, and polysaccharides (5, 36).

Significant amounts of metal sorption can inhibit microbial activity. Recent studies on relationships between metal sorption and microbial toxicity have revealed that inhibition by metals such as Zn, Ni, and Cd is subject to the slow kinetics of metal internalization, while the mechanism of Cu inhibition may involve rapid loss of membrane integrity (10). As noted above, biofilms may be more resistant to toxic metals than planktonic cells, possibly because of retarded metal diffusion into biofilms, which is a result of the adsorption of metals to cell surfaces and metal binding to the extracellular polymers in the biofilm matrix (35).

Recently, biofilm formation under metal stress has been subjected to extensive investigation. While the spatial distributions of oxygen and nitrogen species in biofilms have been successfully determined using microelectrodes (24, 43), few investigations have focused on visualizing the spatial distributions of active biomass and metals in biofilms, largely because of the lack of noninvasive techniques that allow localization over depth. Previous noninvasive techniques for the study of biofilms mainly utilize confocal laser scanning microscopy (CLSM) (7, 35, 42) and are usually limited to penetration depths of up to 100 μm (7, 41).

Two-photon laser scanning microscopy (2P-LSM) offers clear images of material two to three times deeper than that with confocal microscopy (3). In 2P-LSM an ultrafast infrared laser is used to deliver two low-energy photons of sufficient intensity to excite visible fluorescence from a fluorophore. Because the infrared photons are typically absorbed by biological systems much less strongly than are visible photons, this scheme both avoids potential damage to the cells and allows deeper penetration (17). In addition, since two-photon absorption depends quadratically on laser intensity, absorption occurs only at the focus of the laser, so that the technique provides better spatial resolution for imaging of samples (1, 17, 45). Thus, in comparison to single-photon CLSM, two-photon excitation allows reduced phototoxicity and photobleaching, improved spatial localization, and deeper sectioning of samples (26, 41, 45). While applications of 2P-LSM to microbial biofilms are beginning to appear (22, 23), to our knowledge, the advantages of 2P-LSM have yet to be applied to analysis of metal distribution in microbial biofilms.

The goal of this work was to use 2P-LSM to measure and analyze the spatial distributions of metals and active biomass fractions within microbial biofilms. To this end, a specific zinc complexation fluorochrome, 8-hydroxy-5-dimethylsulfoamidoquinoline ($C_{11}H_{12}N_2O_3S$, molecular weight 252, hereafter referred to as quinoline), was synthesized according to previously described methods (25) and used as a marker in the visualization of zinc. A live/dead fluorescent dye mixture (Baclight bacterial viability kit, Molecular Probes, Eugene, OR) was applied to determine bacterial viability.

MATERIALS AND METHODS

Culture and media. The test bacterium was *Escherichia coli* PHL628, a K-12 MG1655 derivative that forms biofilms as a consequence of the overexpression of curli (37). The test strain was grown in a modified minimal mineral salts (MMS) medium (21), which contained, per liter, 0.2 mM $CaCl_2$, 0.14 mM $MgSO_4$, 0.91 mM $(NH_4)_2SO_4$, 0.15 mM KNO_3, 0.01 mM $NaHCO_3$, 0.37 mM KH_2PO_4, and 31 mM pyruvate, with the pH adjusted to 6.0. The MMS medium components have defined Zn binding constants, allowing computation of Zn speciation using chemical equilibrium software such as MINEQL+ (Environmental Research Software; Hallowell, ME) (15, 32). Calculations showed that under the conditions used for the experiments described in this report, mineral precipitation would not occur (assuming added phosphate was consumed by cells) and complexation of Zn was not significant (i.e., the dominant Zn species was the free ion). The solution used to rinse biofilms contained the same components as MMS medium except that no phosphate or pyruvate was added. Thick biofilms were grown in complete Luria-Bertani (LB) medium containing, per liter, 10 g tryptone, 5 g yeast, and 10 g NaCl. All media were sterilized by autoclaving at 121°C before use.

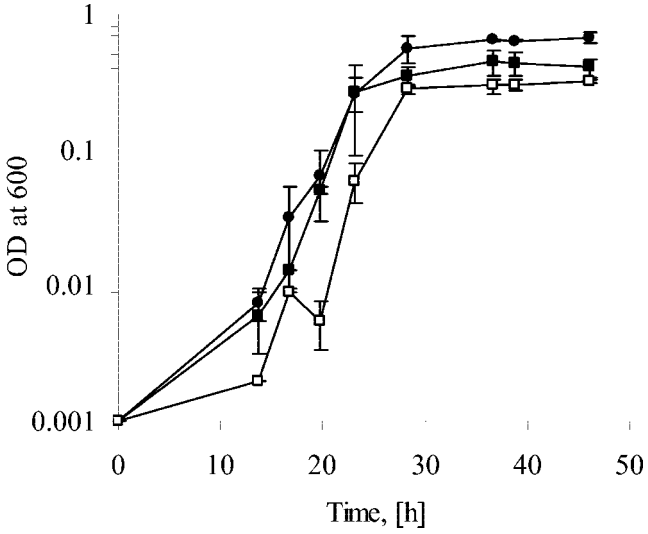

FIG. 1. *E. coli* PHL628 grown in the presence of zinc in MMS medium at 37°C and no Zn (control, ●), 0.1 mM Zn (■), and 1 mM Zn (□).

Biofilms. Thin and thick biofilms were grown under batch and continuous-flow cultivation techniques, respectively (6, 35, 43). Thin biofilms were grown in microwell dishes with 0.17-mm glass coverslips at the bottom (MatTek, Ashland, MA). The microwell dishes were inoculated with 0.5-ml portions of an overnight culture grown in MMS at 37°C, diluted sixfold with the same medium, and incubated on a mechanical shaker (50 rpm) at 30°C. The temperature was changed from 37 to 30°C to facilitate curli overexpression and hence biofilm formation. After 1 to 2 days of incubation, the microwell dishes were washed twice with the MMS rinse solution prior to microscopic examination.

Thick biofilms (up to 350 μm) were grown in a drip-flow culture system (43). Inoculated microwell dishes were kept overnight before the flow containing LB medium was initiated. The LB medium was delivered with a Masterflex peristaltic pump (Cole-Parmer, Vernon Hills, IL) and dripped onto the glass coverslips in microwell dishes at a constant flow rate of 0.08 ml/min at 30°C. After 2 days of continuous feeding, the microwell dishes were washed twice with the MMS rinse solution before staining. Since an open air gap occurred at the point where LB medium was delivered to the dishes, it is possible that the thick biofilms did not remain pure cultures. However, no visual evidence of contamination was observed and, if present, would be unlikely to alter the conclusions regarding the spatial distribution of Zn and active biomass.

Zinc sorption. Suspended cultures of *E. coli* PHL628 cells in early stationary phase (based on the growth curves shown in Fig. 1) were used for both kinetic and isotherm studies. The pH of cultures was adjusted to 7.0 before use. All glassware was acid washed and sterilized prior to use.

Sorption kinetics. Aliquots of concentrated Zn solution (from $ZnCl_2$, pH < 6) were added to the cultures to yield initial concentrations of 0.1 and 1 mM Zn. The cultures were kept at constant temperature (37°C) and continuously mixed on a shaker at 300 rpm. At predetermined intervals (1, 2, 4, 8, and 24 h), aliquots were withdrawn and centrifuged at 20,000 × g for 30 min. Soluble Zn concentrations were determined from the supernatants using an AAanalyst 100 atomic

absorption spectrophotometer (Perkin-Elmer, Norwalk, CT) and the amount of sorbed Zn was calculated from the difference between the initial and measured dissolved Zn concentrations after correction for background values.

Sorption isotherms. Aliquots of Zn stock solution were added to cell cultures to achieve metal doses from 0 to 1.0 mM. Sodium azide was added to one of the cell cultures at a final concentration of 0.15 mM to inhibit microbial activity (20). All samples were incubated under the conditions mentioned above for 1 h (based on the results of the kinetic study), and Zn concentrations in the supernatants were analyzed to determine Zn adsorption isotherms.

Fluorescence measurements. The fluorescence of quinoline and the Zn-quinoline complex was measured with an SLM-8000 fluorometer (SLM Instrument, Urbana, IL). The sample chamber of the fluorometer was maintained at a constant temperature of 25°C with a thermostat-controlled water bath. The fluorescence spectra were measured and analyzed with maximal intensity at excitation and emission wavelengths of 381 and 462 nm, respectively.

To test the effect of Zn on quinoline fluorescence, solutions with or without 50 μM Zn were prepared at pH 6, and aliquots of quinoline were added to yield final concentrations from 0 to 150 μM. Alternatively, the quinoline concentration was held constant at 150 μM while the Zn concentration was varied from 0 to 1 mM.

To evaluate the strength of Zn-quinoline complexation and the efficacy of quinoline in sensing Zn sorbed to biomass, either EDTA, nitrilotriacetate (NTA), citrate, pyruvate, or early-stationary-phase cell cultures (with an assumed molecular formula of $C_5H_7O_2N$) at concentrations ranging from 0 to 220 μM were added as complexing agents along with 100 μM Zn. After 1 h equilibration, aliquots of quinoline were added to yield a final concentration of 150 μM in all samples and incubated for 15 min before fluorescence measurements. For samples with cells, the quinoline-spiked cultures were centrifuged at 20,000 × *g* for 1 min and the supernatants were collected for fluorescence measurements.

Quinoline sorption to suspended and biofilm cultures was evaluated by measuring the fluorescence of quinoline (added at 150 μM) in supernatants after 1 h equilibration in the presence and absence of cells.

Staining. After rinsing twice with the MMS rinse solution, the solution was removed. Thin biofilms on microwell dishes were exposed to 100 μl of 100 μM Zn solution for 1 h. Residual dissolved Zn was removed by washing twice with the MMS rinse solution, and 100 μl of 150 μM quinoline was added and left in the dark for 15 min before being visualized with 2P-LSM. In a similar manner, thick biofilms on microwell dishes were rinsed twice with MMS, the rinse solution was removed, and the biofilm was then exposed to 1 ml of 300 μM Zn solution for 1 h. The cells were then washed twice with the MMS rinse solution, and 1 ml of 300 μM quinoline solution was added. An aliquot (4 μl) of 5 mM SYTO17 (which stains all cells with red fluorescence) (42) was injected immediately (recorded time, 0 min). The biofilm samples were visualized in duplicate at 20-min intervals.

Bacterial cell live/dead distribution was determined by staining with nucleic acid-specific fluorochromes: a green fluorescent nucleic acid stain, SYTO 9 (which stains all cells, live or dead), and a red fluorescent nucleic acid stain, propidium iodide (which stains only bacteria with damaged membranes). A reduction in the SYTO 9 fluorescent emission results when both dyes are present in the cells, and dead cells produce a yellow fluorescence as a result of the combined red and green signals. After rinsing with the MMS rinse solution, the biofilms were stained by adding 3 μl of the dye mixture per ml solution according to the manufacturer's protocols. The stained samples were left in the dark for 15 min before microscopic visualization.

Microscopic imaging and data processing. A Bio-Rad 1024 confocal/2P-LSM microscope system was used for imaging. The system for 2P-LSM is equipped with a Ti:Sapphire mode-locked laser, which provides 100-fs pulses at 80 MHz. The microscope system also contains three fluorescence emission detectors, an Olympus IX70 inverted microscope with a 100× oil-immersion objective, a Z-motor that allows a series of sections to be taken automatically, a Marzhuaser X-Y motorized stage for image location, and LaserSharp software for image acquisition. Images were further processed and analyzed using Confocal Assistant software (downloaded from ftp.genetics.Bio-Rad.com) and Scion (from NIH Image, http://www.scioncorp.com).

The percentage of active biomass was inferred from the difference between the measured average gray values (AGV) of images from live (green) (AGV_g) and dead (red) (AGV_r) staining as follows: % active fraction = $[AGV_g/(AGV_g + AGV_r)] \times 100$.

RESULTS

Bacterial growth curves. The growth of planktonic *E. coli* PHL628 cells in MMS medium at 37°C reached early stationary phase after 24 h of cultivation (Fig. 1). Based on the growth curves, an overnight cultivation was carried out prior to each experiment to provide uniform inocula for biofilm growth. No significant lag phase was observed in the presence of 0.1 mM Zn, but cell growth was mildly retarded in the presence of 1 mM Zn, indicating that Zn had limited toxicity for planktonic bacterial growth.

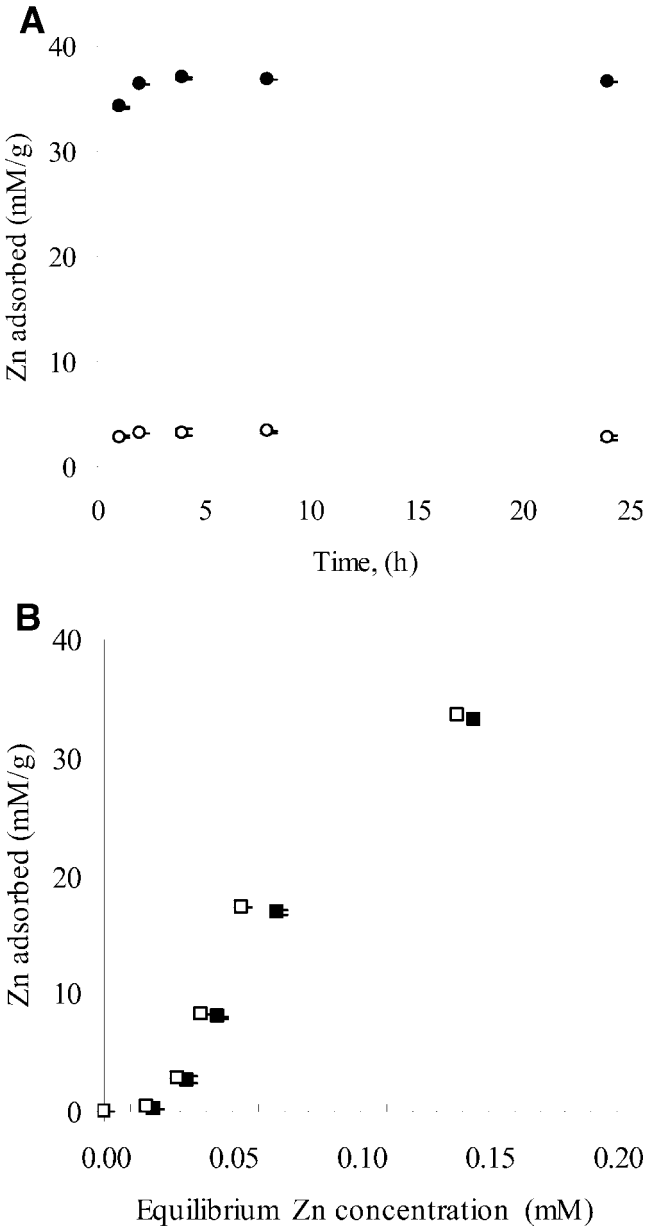

FIG. 2. Zn adsorption to planktonic *E. coli* PHL628 cells at pH 7. (A) Zn adsorption kinetics at 30°C with 0.1 mM Zn (○) and 1 mM Zn (●). (B) Zn sorption isotherms with active (■) and inactive (□) (0.15 mM NaN_3-treated) cells at 37°C.

Zn sorption to planktonic bacteria. Zn sorption kinetics and equilibria were evaluated using planktonic cells harvested in stationary phase. As was expected, Zn sorption to planktonic cells was fast (within an hour), and sorbed Zn remained constant as the incubation time increased from 1 to 24 h (Fig. 2A).

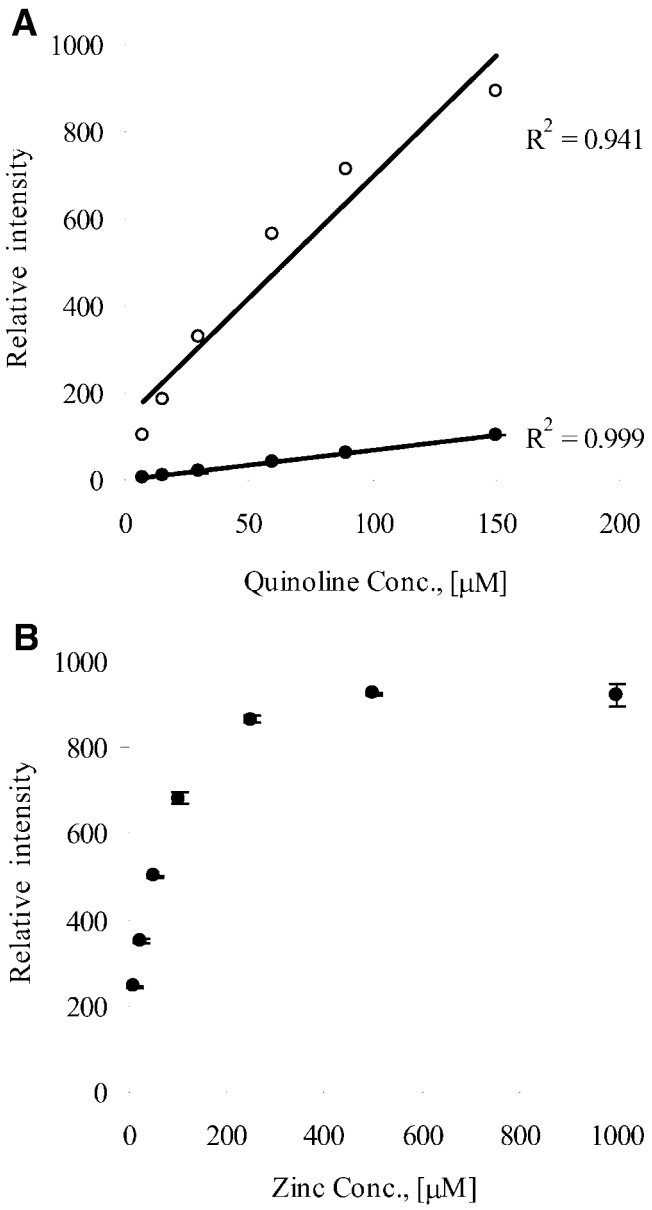

FIG. 3. (A) Fluorescence intensity as a function of quinoline concentration in the presence (○) and absence (●) of 50 μM Zn. (B) Fluorescence intensity as a function of Zn concentration in the presence of 150 μM quinoline.

Zn sorption to biomass obeyed a linear isotherm up to 0.07 mM Zn (Fig. 2B). Based on mass balance analysis, most of the added Zn (80 to 93%) was sorbed to biomass at a cell concentration of 25.8 mg/liter. It appeared that the amount of Zn sorbed to the inactive biomass was significantly higher (t_α = 0.05, $P < 0.04$, $n = 4$) than that of Zn sorbed to the active biomass.

Evaluation of fluorochrome. The synthesized quinoline fluorochrome specifically bound zinc (Fig. 3A) but not other test metals such as copper and lead (data not shown). Zn addition increased quinoline fluorescence intensity by 9- to 20-fold (Fig. 3A). Based on the molar ratio of quinoline to added Zn, it appeared that the synthesized quinoline was capable of forming up to 3:1 complexes with Zn^{2+} (3 mol quinoline to 1 mol Zn), similar to other quinoline-based Zn chelators (8, 25) (Fig. 3A and 3B). 8-Hydroxy-quinoline can form both 1:1 and 2:1 complexes with Zn^{2+} (depending on pH and solvent). At the physiological pH of approximately 7, both 1:1 and 2:1 complexes are likely to be present in solution (2).

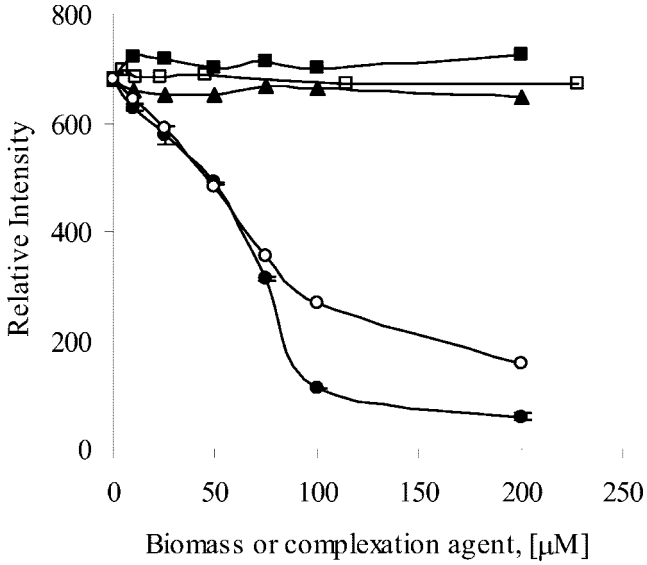

FIG. 4. Effect of biomass and complexing agents on Zn-quinoline fluorescence intensity, including EDTA (●), NTA (○), citrate (■), cell cultures (□), and pyruvate (▲).

A series of complexing agents and *E. coli* PHL628 cell cultures was selected to determine whether complexed and cell-bound Zn species were labile with the addition of quinoline. Zn strongly complexes with EDTA, with a first-step Zn-EDTA formation constant (log K_f) of 18.3. As Zn^{2+} was complexed with more EDTA, less Zn-quinoline fluorescence was detected (Fig. 4). Similar results were obtained for NTA, although the decrease in total fluorescence was less than that seen with EDTA. This is not surprising given the lower binding strength of NTA (log K_f = 12.0) relative to EDTA. Zn and citrate formed a weak complex (log K_f = 6.1) that had no effect on the Zn-quinoline fluorescence measurements. This was also the case for solutions containing pyruvate and cell cultures, indicating that Zn adsorbed to biomass was labile and could be rapidly (<15 min) desorbed and complexed by the quinoline.

Spatial distribution of Zinc in biofilms. Biofilm development was investigated using both batch and continuous-flow cultivation techniques. In general, thin biofilms were developed in the batch conditions, with typical thicknesses of 10 to 50 μm after 1 to 2 days of cultivation. In comparison, thick biofilms (up to 350 μm in this study) were obtained only in the continuous-flow conditions with LB medium.

After application of the SYTO 9 and propidium iodide stains in the absence of Zn, thin biofilms fluoresced green (a few cells close to the substratum fluoresced yellow), indicating that the preponderance of cells in the thin biofilms were viable and metabolically active (Fig. 5A and C). The thick biofilms contained dispersed, brightly fluorescent cell clusters (Fig. 5A) with horizontally oriented dark areas, which we presumed to be voids that allow fluid flow (Fig. 5B). As expected, the bio-

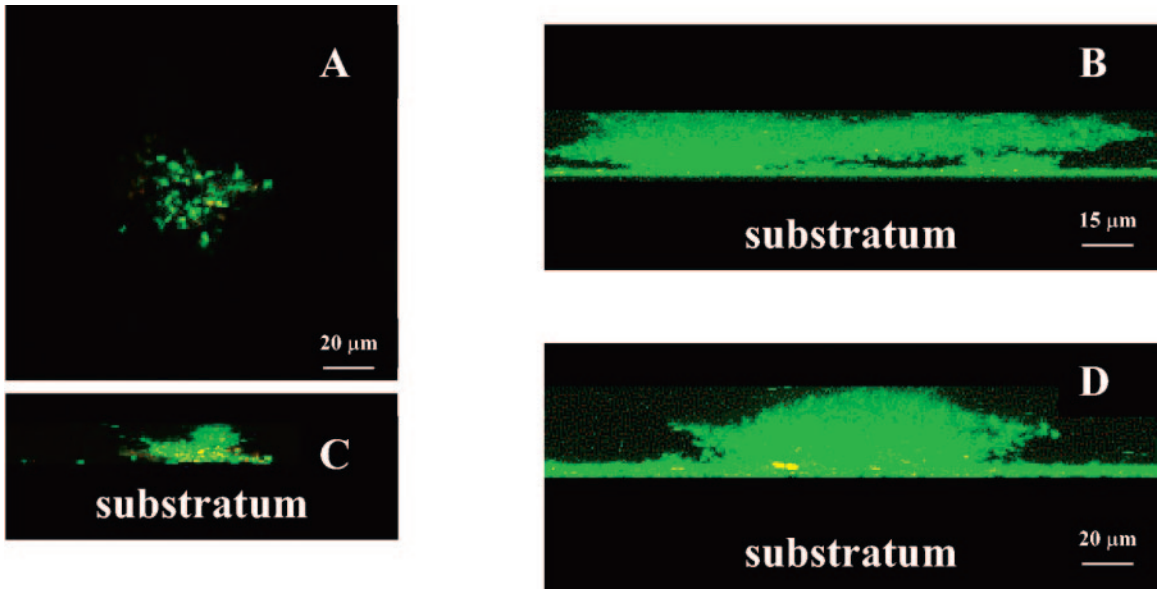

FIG. 5. Photomicrographs of *E. coli* PHL628 biofilms grown in MMS medium using pyruvate as the carbon and energy source in the absence of zinc at 30°C. (A and C) Biofilms in the absence of Zn. (A) Top-down view (4 μm away from the substratum). (C) Cross-sectional view of the biofilm from A with the substratum at the bottom. (B) Cross-sectional view of a biofilm showing fluid channels. (D) Cross-sectional view of a biofilm with nonuniform structures. Dead (inactive) cells were stained red with propidium iodide; live (active) cells were stained green with SYTO9.

film images showed irregular edges (Fig. 5C and D), which indicate the complex three-dimensional structure of the biofilm.

Zn additions were distributed quite evenly in the thin biofilms (12 μm) (Fig. 6A and B). In contrast, Zn was located only at the surface of thick biofilms, with a penetration depth of less than 20 μm (Fig. 7A). The results of intensity estimates showed that duplicates were similar (Fig. 7B has a mean gray value of 38.52 versus that of 38.33 in Fig. 7A). The signal from the penetration of Zn into the biofilm was significantly reduced after 20 min of reaction with the quinoline (Fig. 7C), and the Zn distribution could not be observed after 40 min (Fig. 7D). The gradual reduction in the Zn signal with time after the addition of quinoline was attributed to diffusion of the Zn-quinoline complex out of the biofilm.

Spatial distribution of active biomass in biofilms. The active biomass in biofilms, as indicated by live (active)/dead (inactive) staining, was dependent upon biofilm thickness. In a 36-μm-

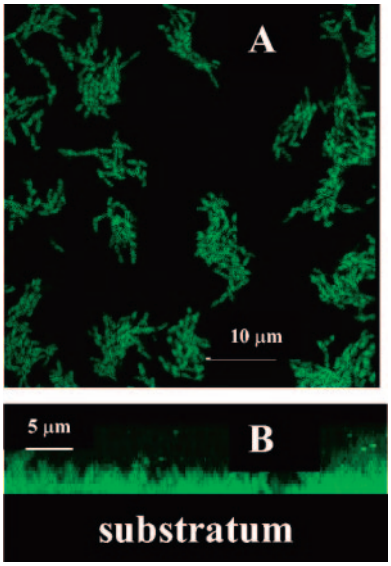

FIG. 6. Photomicrographs of *E. coli* PHL628 biofilms grown in MMS medium at 30°C after Zn treatment. An aliquot of Zn (100 μM) was added 1 h before staining. Zn in the biofilms was stained blue with 150 μM quinoline. The blue fluorescence has been replaced with the false color green to improve contrast in the image. (A) Top-down view (2.5 μm away from the substratum). (B) Side view with the substratum at the bottom.

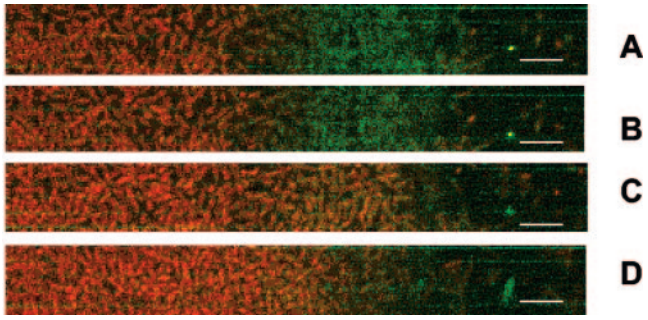

FIG. 7. Zn distribution in *E. coli* PHL628 biofilms grown in LB medium at 30°C. An aliquot of Zn (300 μM) was added 1 h before staining. Zn in the biofilms was stained blue with 300 μM quinoline, and all cells in the biofilms were stained red with SYTO 17. (A) The blue fluorescence has been replaced with the false color green to improve contrast in the image. Top-down view with the biofilm surface on the right at time zero (immediately after the addition of both dyes). (B) Top-down view at time zero (duplicate with a few minutes delay compared to A). (C) Top-down view after 20 min. (D) Top-down view after 40 min. Bars, 10 μm.

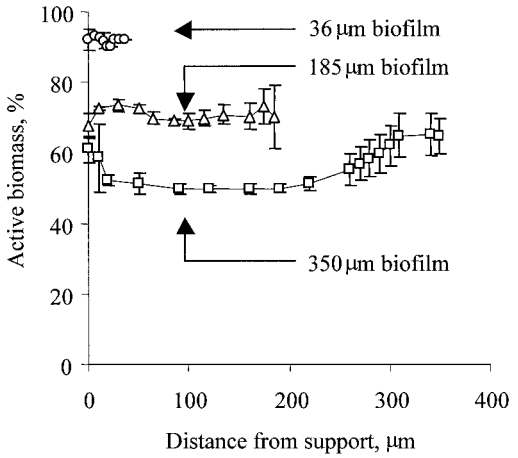

FIG. 8. Distribution of active biomass in a series of *E. coli* PHL628 biofilms. The 36-μm biofilm was grown in MMS medium at 30°C under batch conditions. The 185-μm and 350-μm biofilms were both grown in LB medium at 30°C under continuous-drip flow conditions.

thick biofilm, more than 90% of the total biomass was active and uniformly distributed (Fig. 5 and 8); but a nonuniform distribution of active biomass was observed in a 185-μm biofilm, where the active fractions varied between 67.7% and 73.6%, with an average of 70.7 ± 1.9% throughout the biofilm structure (Fig. 8). When the thickness of the biofilm increased to 350 μm, 61.0 ± 3.7% of the biomass was active at the substratum. The active biomass decreased with distance up to 20 μm away from the substratum. Between 20 and 220 μm from the substratum, active biomass was at a relatively constant low level (50.6 ± 1.0%) and then gradually increased back to 64.7 ± 4.9% close to the biofilm surface.

DISCUSSION

Several Zn chelators based on a quinoline core, such as 6-methoxy-(8-*p*-toluenesulfonamido)-quinoline, have been developed for imaging of biological samples (8, 38). These zinc-activated fluorochromes are usually capable of permeating the cell, with moderately strong Zn complexation (first-step log K_f values ranged from 7 to 8.4) (8, 38). The pZn values ($-\log [Zn^{2+}]$) for EDTA and the quinoline-based fluorochromes are 14.3 and 9.3, respectively) (8). Hence, quinoline-based fluorochromes could not readily bind Zn species that were complexed with EDTA (Fig. 4), but they were efficient in removing Zn that was sorbed to biomass. The constant for Zn binding to *E. coli* PHL628 cell surfaces is likely to be comparable in magnitude to that of Cd complexation with bacterial surfaces ($\log K_f = 4.0$) (44).

With the experimental protocol used in this research, the sequence of Zn-quinoline interactions within a biofilm include the following: Zn diffusion into and sorption to the biofilm; quinoline diffusion into the biofilm; Zn desorption in the presence of quinoline; and diffusion of the Zn-quinoline complex out of the biofilm. Quinoline was confirmed to have no sorption to suspended and biofilm cell cultures by comparing its fluorescence in the presence and absence of cells (data not shown). Metal sorption to biomass has been confirmed to be a rapid process, as shown before (10, 18) as well as in this work. Quinoline-induced Zn desorption from biomass also happened on a rapid time scale. The diffusion of nonreacting solutes (such as quinoline and the Zn-quinoline complexes) within a biofilm occurs on a time scale ranging from seconds to tens of minutes, depending on the biofilm thickness (33). However, diffusion of metal ions, such as Zn^{2+}, into the biofilm will be retarded by binding to cells and extracellular polymers and is expected to be much slower than the other processes noted above. Thus, observations of the spatial distribution of metals using the methods described here need to be performed quickly (within minutes) relative to the time scale for movement of Zn that has desorbed from the biofilm in response to the presence of the quinoline ligand.

Our results are consistent with those from a recent study that showed significant levels of viable cells in the interior regions of a 10-μm *Pseudomonas aeruginosa* biofilm after 12 h of treatment with 1 mM copper (35). Although the research reported here did not allow us to quantify the Zn concentration gradient in the biofilm (in part because of the bleedthrough of SYTO 17 red fluorescence into the blue channel), our results clearly show that after 1 h of equilibration, Zn is mainly located in the biofilm surface with a penetration depth of less than 20 μm (Fig. 7). The slow penetration (hindered diffusion) of Zn inside the biofilm structure versus the fast sorption of Zn to the biofilm matrix will enhance the survival of cells in a biofilm under metal stress compared to planktonic cells.

Our results further suggest that total microbial activity decreases with increasing depth of the biofilm (Fig. 8). The lower active fraction of cells at the surface of the 185- and 350-μm biofilms (versus the 36-μm biofilm) may have been due to the reduced oxygen concentration and/or the accumulation of waste products that would likely accompany the observed cell density; direct measurements of oxygen and waste products were not made, however. Furthermore, a U-shaped distribution of active biomass was observed in a 350-μm biofilm, suggesting that the middle part of the biofilm is less active than either the top (e.g., the biofilm-bulk liquid interface) or the bottom (substratum), perhaps as a result of limited advective transport. However, the significant amount of active biomass distributed all over the thick biofilms suggests that essential nutrients, electron donors, and electron acceptors are still available to biomass in the inner biofilm regions. Thus, our results do not support predictions based on the concept of homogeneous biofilm models with active biomass located predominantly near the interface of the biofilm and the bulk aqueous phase and inactive biomass in the inner regions (27, 30, 39).

Given our current understanding, confirmed in this study, that biofilms are heterogeneous spatial structures consisting of dense cell clusters (Fig. 5) (11), with open spaces between the clusters, biofilm models are required that permit mass transport through both diffusion within cell clusters and advection in the open channels that penetrate the biofilms. Further work is needed to build a mechanistic model with an appropriate geometric description, in which the combined transport processes of advection and diffusion are accounted for, to better predict the spatial distribution of biochemical processes in biofilms.

Previous work and this research confirm many advantages of

2P-LSM compared to single-photon CLSM in studies of interfacial microbial ecology, including reduced photobleaching and the ability to analyze thick films (26, 45). In single-photon CLSM, quinoline-based fluorescence probes will require UV excitation at 350 to 380 nm, and this wavelength is below the range commonly available in single-photon instruments. More importantly, shorter wavelengths in the UV range have higher energy and consequently can be damaging to cells (38). Photobleaching is significantly reduced in 2P-LSM, where two photons are used to excite the fluorochrome of interest (the Ti-Sapphire infrared laser used in this work provided light at 790 nm). The biofilm penetration in this work was sufficient to permit analysis of *E. coli* PHL628 biofilms with thicknesses as great as 350 μm.

The fact that the amount of Zn sorbed to the inactive biomass was slightly higher than that sorbed to the active biomass (Fig. 2) indicates the possible involvement of a Zn homeostasis mechanism that regulates the uptake and efflux of zinc in the microbial system. In *E. coli*, high concentrations of zinc are reported to result in zinc efflux by induction of ZntA, a zinc-transporting P-type ATPase (28, 29). With 2P-LSM and a judicious choice of fluorochromes, it is possible to simultaneously visualize the localization of intracellular and extracellular Zn and the cell activity level. Although the results presented suggest that the levels of Zn used were not toxic, more work is needed to determine the actual bioavailability of metals within the biofilm and what role cellular processes, including exopolysaccharide production and metal efflux, play in reducing toxicity. Research of this nature would greatly augment our understanding of the function of microbial biofilms under metal stress.

ACKNOWLEDGMENTS

This research was supported, in part, by NSF grant number EAR-0311767. Z.H. is a postdoctoral fellow with support provided by the Cornell Biocomplexity and Biogeochemistry Initiative.

We appreciate the assistance of Carol Bayles from the Nanobiotechnology Center (NBTC) at Cornell University and acknowledge the use of NBTC's shared facilities (NSF STC, ECS-9876771). *E. coli* PHL628 was a gift from Philippe Lajeune. We also thank Stefan Bernhard and Jay C. Henderson for providing the quinoline compound.

REFERENCES

1. **Albota, M., D. Beljonne, J. L. Bredas, J. E. Ehrlich, J. Y. Fu, A. A. Heikal, S. E. Hess, T. Kogej, M. D. Levin, S. R. Marder, D. McCord-Maughon, J. W. Perry, H. Rockel, M. Rumi, C. Subramaniam, W. W. Webb, X. L. Wu, and C. Xu.** 1998. Design of organic molecules with large two-photon absorption cross sections. Science **281:**1653–1656.
2. **Bishop, E. (ed.).** 1972. Indicators. Pergamon Press, Braunschweig, Germany.
3. **Centonze, V. E., and J. G. White.** 1998. Multiphoton excitation provides optical sections from deeper within scattering specimens than confocal imaging. Biophys. J. **75:**2015–2024.
4. **Costerton, J. W., G. G. Geesey, and G. K. Cheng.** 1978. How bacteria stick. Sci. Am. **238:**86–95.
5. **Cox, J. S., D. S. Smith, L. A. Warren, and F. G. Ferris.** 1999. Characterizing heterogeneous bacterial surface functional groups using discrete affinity spectra for proton binding. Environ. Sci. Technol. **33:**4514–4521.
6. **De Kievit, T. R., R. Gillis, S. Marx, C. Brown, and B. H. Iglewski.** 2001. Quorum-sensing genes in *Pseudomonas aeruginosa* biofilms: their role and expression patterns. Appl. Environ. Microbiol. **67:**1865–1873.
7. **Eaglesham, B. S., L. W. Lion, and W. C. Ghiorse.** 2003. An Aufwuchs chamber slide for high-resolution confocal laser scanning microscopy and stereo imaging of microbial communities in natural biofilms. Microb. Ecol. **47:**266–270.
8. **Fahrni, C. J., and T. V. O'Halloran.** 1999. Aqueous coordination chemistry of quinoline-based fluorescence probes for the biological chemistry of zinc. J. Am. Chem. Soc. **121:**11448–11458.
9. **Grady, C. P. L., G. T. Daigger, and H. C. Lim.** 1999. Biological wastewater treatment, 2nd ed. Marcel Dekker, New York, N.Y.
10. **Hu, Z., K. Chandran, D. Grasso, and B. F. Smets.** 2003. Impact of heavy metal sorption and internalization on nitrification inhibition. Environ. Sci. Technol. **37:**728–734.
11. **Kuehn, M., M. Hausner, H.-J. Bungartz, M. Wagner, P. A. Wilderer, and S. Wuertz.** 1998. Automated confocal laser scanning microscopy and semiautomated image processing for analysis of biofilms. Appl. Environ. Microbiol. **64:**4115–4127.
12. **Langley, S., and T. J. Beveridge.** 1999. Metal binding by *Pseudomonas aeruginosa* PAO1 is influenced by growth of the cells as a biofilm. Can. J. Microbiol. **45:**616–622.
13. **Lawrence, J. R., G. D. W. Swerhone, G. G. Leppard, T. Araki, X. Zhang, M. M. West, and A. P. Hitchcock.** 2003. Scanning transmission x-ray, laser scanning, and transmission electron microscopy mapping of the exopolymeric matrix of microbial biofilms. Appl. Environ. Microbiol. **69:**5543–5554.
14. **Lazarova, V., and J. Manem.** 1995. Biofilm characterization and activity analysis in water and wastewater treatment. Water Res. **29:**2227–2245.
15. **Martell, A. E., and R. M. Smith.** 1977. Critical stability constants, vol. 3. Plenum Press, New York, N.Y.
16. **Meyer, B.** 2003. Approaches to prevention, removal and killing of biofilms. Int. Biodeterior. Biodegrad. **51:**249–253.
17. **Nakamura, O.** 1999. Fundamental of two-photon microscopy. Microsc. Res. Technol. **47:**165–171.
18. **Nelson, P. O., A. K. Chung, and M. C. Hudson.** 1981. Factors affecting the fate of heavy metals in the activated sludge process. J. Water Pollut. Control Fed. **53:**1323–1333.
19. **Nelson, Y. M., L. M. Lion, M. L. Shuler, and W. C. Ghiorse.** 1996. Modeling oligotrophic biofilm formation and lead adsorption to biofilm components. Environ. Sci. Technol. **30:**2027–2035.
20. **Nelson, Y. M., L. W. Lion, W. C. Ghiorse, and M. L. Shuler.** 1999. Production of biogenic Mn oxides by *Leptothrix discophora* SS-1 in a chemically defined growth medium and evaluation of their Pb adsorption characteristics. Appl. Environ. Microbiol. **65:**175–180.
21. **Nelson, Y. M., W. Lo, L. M. Lion, M. L. Shuler, and W. C. Ghiorse.** 1995. Lead distribution in a simulated aquatic environment-effects of bacterial biofilms and iron-oxide. Water Res. **29:**1934–1944.
22. **Neu, T. R., U. Kuhlicke, and J. R. Lawrence.** 2002. Assessment of fluorochromes for two-photon laser scanning microscopy of biofilms. Appl. Environ. Microbiol. **68:**901–909.
23. **Neu, T. R., S. Woelfl, and J. R. Lawrence.** 2004. Three-dimensional differentiation of photo-autotrophic biofilm constituents by multi-channel laser scanning microscopy (single-photon and two-photon excitation). J. Microbiol. Methods **56:**161–172.
24. **Okabe, S., H. Satoh, and Y. Watanabe.** 1999. In situ analysis of nitrifying biofilms as determined by in situ hybridization and the use of microelectrodes. Appl. Environ. Microbiol. **65:**3182–3191.
25. **Pearce, D. A., N. Jotterand, I. S. Carrico, and B. Imperiali.** 2001. Derivatives of 8-hydroxy-2-methylquinoline are powerful prototypes for zinc sensors in biological systems. J. Am. Chem. Soc. **123:**5160–5161.
26. **Periasamy, A., P. Skoglund, C. Noakes, and R. Keller.** 1999. An evaluation of two-photon excitation versus confocal and digital deconvolution fluorescence microscopy imaging in Xenopus morphogenesis. Microsc. Res. Technol. **47:**172–181.
27. **Rauch, W., H. Vanhooren, and P. A. Vanrolleghem.** 1999. A simplified mixed-culture biofilm model. Water Res. **33:**2148–2162.
28. **Rensing, C., M. Ghosh, and B. P. Rosen.** 1999. Families of soft-metal-ion-transporting ATPases. J. Bacteriol. **181:**5891–5897.
29. **Rensing, C., B. Mitra, and B. P. Rosen.** 1997. The zntA gene of *Escherichia coli* encodes a Zn(II)-translocating P-type ATPase. Proc. Natl. Acad. Sci. USA **94:**14326–14331.
30. **Rittmann, B. E., and J. A. Manem.** 1992. Development and experimental evaluation of a steady-state, multispecies biofilm model. Biotechnol. Bioeng. **39:**914–922.
31. **Rittmann, B. E., D. Stilwell, and A. Ohashi.** 2002. The transient-state, multiple-species biofilm model for biofiltration processes. Water Res. **36:**2342–2356.
32. **Schecher, W. D., and D. C. McAvoy.** 2001. MINEQL+: a chemical equilibrium modeling system. Version 4.5 for Windows. Environmental Research Software, Hallowell, Maine.
33. **Stewart, P. S.** 2003. Diffusion in biofilms. J. Bacteriol. **185:**1485–1491.
34. **Stoodley, P., K. Sauer, D. G. Davies, and J. W. Costerton.** 2002. Biofilms as complex differentiated communities. Annu. Rev. Microbiol. **56:**187–209.
35. **Teitzel, G. M., and M. R. Parsek.** 2003. Heavy metal resistance of biofilm and planktonic *Pseudomonas aeruginosa*. Appl. Environ. Microbiol. **69:**2313–2320.
36. **Texier, A., Y. Andres, M. Illemassene, and P. L. Cloirec.** 2000. Characterization of lanthanide ions binding sites in the cell wall of *Pseudomonos aeruginosa*. Environ. Sci. Technol. **34:**610–615.
37. **Vidal, O., R. Longin, C. Prigent-Combaret, C. Dorel, M. Hooreman, and P. Lejeune.** 1998. Isolation of an *Escherichia coli* K-12 mutant strain able to form biofilms on inert surfaces: involvement of a new *ompR* allele that increases curli expression. J. Bacteriol. **180:**2442–2449.

38. **Walkup, G. K., S. C. Burdette, S. J. Lippard, and R. Y. Tsien.** 2000. A new cell-permeable fluorescent probe for Zn^{2+}. J. Am. Chem. Soc. **122:**5644–5645.
39. **Wanner, O., and W. Gujer.** 1984. Competition in biofilms. Water Sci. Technol. **17:**27–44.
40. **Watnick, P., and R. Kolter.** 2000. Biofilm, city of microbes. J. Bacteriol. **182:**2675–2679.
41. **Williams, R. M., W. R. Zipfel, and W. W. Webb.** 2001. Multiphoton microscopy in biological research. Curr. Opin. Chem. Biol. **5:**603–608.
42. **Wuertz, S., E. Muller, R. Spaeth, P. Pfleiderer, and H.-C. Flemming.** 2000. Detection of heavy metals in bacterial biofilms and microbial flocs with the fluorescent complexing agent Newport Green. J. Ind. Microbiol. Biotechnol. **24:**116–123.
43. **Xu, K. D., P. S. Stewart, F. Xia, C.-T. Huang, and G. A. McFeters.** 1998. Spatial physiological heterogeneity in *Pseudomonas aeruginosa* biofilm is determined by oxygen availability. Appl. Environ. Microbiol. **64:**4035–4039.
44. **Yee, N., and J. Fein.** 2001. Cd adsorption onto bacterial surfaces: a universal adsorption edge? Geochim. Cosmochim. Acta **65:**2037–2042.
45. **Zipfel, W. R., R. M. Williams, and W. W. Webb.** 2003. Nonlinear magic: multiphoton microscopy in the biosciences. Nat. Biotechnol. **21:**1369–1377.